2021

Differentiating early from later diagenesis Cretaceous sandstone and petroleum reservoir of the Cedar Mountain Formation in Utah

C. Robertson

G.A. Ludvigson

R.M. Joeckel
University of Nebraska - Lincoln

S. Mohammadi

J.I. Kirkland

Differentiating early from later diagenesis in a Cretaceous sandstone and petroleum reservoir of the Cedar Mountain Formation, Utah

Clay Robertson[1], Greg A. Ludvigson[2*], R.M. Joeckel[3], Sahar Mohammadi[2], and James I. Kirkland[4]

[1]Department of Geology, University of Kansas, Ritchie Hall, Earth, Energy & Environment Center, 1414 Naismith Dr., Lawrence, KS 66045-7575

[2]Kansas Geological Survey, University of Kansas, 1930 Constant Ave., Lawrence, KS 66047-3724

[3]Conservation and Survey Division, School of Natural Resources, University of Nebraska–Lincoln, 615 S. Hardin Hall, 3310 Holdrege St., Lincoln, NE 68583-0996

[4]Utah Geological Survey, 1594 W. North Temple, Suite 3110, Salt Lake City, UT 84114

[*]Correspondence should be addressed to: gludvigson@ku.edu

ABSTRACT

Previously published anomalous whole-rock stable isotopic values from the Poison Strip Sandstone Member of the Cretaceous Cedar Mountain Formation (CMF) of eastern Utah are of uncertain origins. This study investigated the diagenetic history and the processes responsible for these anomalous data. Accordingly, we integrated photomicroscopic techniques including polarized light microscopy, epifluorescence and cathodoluminescence (CL) imaging, micromilling of stable isotope samples, and fluid-inclusion heating and freezing measurements to this end. The key observations involved the microscopic mapping of calcite cement stratigraphy using CL imaging to permit the analysis of stable isotopes of calcite cements that crystallized during early and late diagenesis. The mapping of calcite cement zones of sufficient submillimeter size to mill out and isolate microgram-sized stable isotope samples enabled this discrimination. Early diagenetic calcite cements have the most positive $\delta^{18}O$ values (-10 to -8.5‰ Vienna Pee Dee Belemnite [VPDB]) of all components. The pattern of $\delta^{13}C$ and $\delta^{18}O$ variation in this early diagenetic cement indicates affinities with early meteoric diagenesis previously documented in published literature on the CFM. The late diagenetic calcite cements yield the most negative $\delta^{18}O$ values (-18 to -16‰ VPDB). We interpret the late diagenetic cements to be responsible for the anomalously low whole-rock $\delta^{18}O$ values previously reported from the Poison Strip Sandstone Member. Our discoveries of bitumen in late-stage pore fillings and liquid petroleum in the fluid inclusions of late diagenetic calcite cements of the Poison Strip Sandstone Member explain the lower whole-rock organic matter $\delta^{13}C$ values and anomalous $\Delta^{13}C$ values reported from the unit. Comparatively lower carbonate $\delta^{18}O$ and organic $\delta^{13}C$ values originally derived from whole-rock analyses of samples from the Poison Strip Sandstone Member resulted from high-temperature basinal diagenesis (hydrothermal circulation and/or petroleum migration), rather than the alternative interpretation of early diagenesis related to a Cretaceous paleoclimatic perturbation. Our results are illustrative of methods to resolve the long-standing geologic problem of discriminating and characterizing products of early vs. late diagenesis in terrigenous clastic sedimentary strata.

KEY WORDS: Cedar Mountain Formation, Cretaceous, diagenesis, fluid-inclusion data, Poison Strip Sandstone Member, stable isotope data.

INTRODUCTION

The Cretaceous Cedar Mountain Formation (CMF) of eastern Utah is a widely recognized focus of research activity as an archive of the terrestrial record of early Cretaceous global change (Ludvigson et al., 2010, 2015; C. Suarez et al., 2014, 2020; M. Suarez et al., 2020). Studies of the CMF (Berriasian–Albian) on the east side of the San Rafael Swell have provided important $\delta^{13}C$ and $\delta^{18}O$ chemostratigraphic data, U–Pb radiometric dates, vertebrate faunas, and palynomorph assemblages. It has also provided the means for interpreting Cretaceous ter-

restrial paleoclimates, depositional systems, and paleoenvironments in present western North America (e.g., Kirkland et al., 1997, 2016a, 2016b; Ludvigson el al., 2010, 2015; C. Suarez et al., 2014, 2020; Joeckel et al., 2017, 2019; M. Suarez et al., 2017, 2020). Although stable isotopic data from multiple mineral substrates in the CMF have previously been published, this paper is the first to resolve multiple diagenetic effects through the use of calcite cement stratigraphy, thus placing those effects in a temporal context.

Anomalously low whole-rock carbonate $\delta^{18}O$ values of -16.0 to -13.5‰ relative to the Vienna Pee Dee Belemnite (VPDB) isotope standard from sandstones of the Poison Strip Sandstone Member of the CMF at the Ruby Ranch Road locality (Fig. 1; see Ludvigson et al., 2015, their fig. 10) are markedly different from two distinct subsets of calcite $\delta^{18}O$ values previously published from the CMF: (1) calcite cement $\delta^{18}O$ values of approximately -8.0‰ VPDB are relatable to early meteoric diagenesis; and (2) vein-calcite $\delta^{18}O$ values of -11.0 to -9.0 VPDB likely formed during burial (Ludvigson et al., 2010, 2015). Another important paleoclimate indicator, the $\Delta^{13}C$ paleo-pCO_2 proxy (carbonate $\delta^{13}C$ values - organic $\delta^{13}C$ values) yields problematic results in the Poison Strip Sandstone Member (Fig. 1; hereafter referred to as the 'Poison Strip Member'). The $\Delta^{13}C$ values from sedimentary rocks are a critical parameter in transfer functions to calculate ancient pCO_2 values. We here consider the two alternative ideas posed by Ludvigson et al. (2015) to explain the origins of the anomalously low whole-rock carbonate $\delta^{18}O$ values and organic $\delta^{13}C$ values from the Poison Strip Member.

Depositional or Late Diagenetic Controls on Whole-Rock Oxygen Isotope Values?

One idea is that the whole-rock carbonate $\delta^{18}O$ data from the Poison Strip Member result from authigenic processes during an Early Cretaceous paleoclimatic perturbation, such as a deglaciation in the nearby Sevier orogenic highlands (see Ludvigson et al., 2015, their fig. 3). The anomalously low $\delta^{18}O$ values in the Poison Strip Member are similar to those reported from well-preserved Early and Late Cretaceous unionid bivalves that inhabited ancient rivers presumed to have carried some ancient alpine snowmelt (Glancy et al., 1993; Dettman and Lohmann, 2000). An alternative idea is that that the anomalous $\delta^{18}O$ values result from much later, higher-temperature basinal diagenetic processes under burial conditions, directly related to either late-stage hydrothermal circulation and/or petroleum migration. This concept relates to the well-documented observation that burial diagenetic processes yield much lower carbonate $\delta^{18}O$ values than those of earlier authigenic carbonates (Choquette and James, 1987; Algeo et al., 1992; Hasiuk et al., 2016).

Depositional or Late Diagenetic Controls on Whole-Rock Organic Carbon Isotope Values?

The lower organic matter $\delta^{13}C$ values in the coarse-grained Poison Strip Member could possibly be related to the particulate organic matter inputs from C3 terrestrial vegetation of alpine paleoenvironments from higher elevations in the drainage basin. This organic matter could have differed from the more water-stressed lowland paleofloras characteristic of the remainder of the CMF. Lower $\delta^{13}C$ values in C3 plants are associated with lower temperatures and higher relative humidities, both of which are compatible with alpine environments (Edwards et al., 2000). Water-stressed lowland paleofloras of the CMF (Ludvigson et al., 2015; Joeckel et al., 2017) could possibly have included crassulacean acid metabolism (CAM) plants with higher $\delta^{13}C$ values than C3 plants, considering speculations about the appearance of CAM during the Mesozoic (Ehleringer and Monson, 1993). The $\delta^{13}C$ values of authigenic carbonates throughout the CMF are interpreted to have been controlled by changes in paleoatmospheric $\delta^{13}C$ values (Ludvigson et al., 2010, 2015; M. Suarez et al., 2020). Therefore, changes in the type of organic matter and the lower organic $\delta^{13}C$ values in the Poison Strip Member would give rise to the anomalous $\Delta^{13}C$ values in the unit. An alternative idea is that organic matter with lower $\delta^{13}C$ values might have been introduced into the Poison Strip Member during later diagenetic processes under burial conditions. For example, migrated petroleum could alter the original depositional whole-rock $\Delta^{13}C$ values in the Poison Strip Member.

The scientific results presented here address the lingering questions posed by the published whole-rock chemostratigraphic profile of the CMF at the Ruby Ranch Road section. An important goal of presenting these research methods and results is to provide an example of the framework for deconvolving early diagenesis from later alteration, and differentiating these products and processes in ancient terrestrial stratigraphic successions.

GEOLOGIC SETTING

The Cedar Mountain Formation (CMF) is a distinct interval of continental sedimentary strata divided into six members in eastern Utah and westernmost Colorado (Kirkland et al., 2016b). The Poison Strip Member is underlain by the Yellow Cat Member—the basal member of the CMF that only occurs between the Green and Colorado rivers in Utah (Kirkland et al., 2016b; Joeckel et al., 2017, 2019). The Poison Strip Member is overlain by the more widespread Ruby Ranch Member across a large part of the Colorado Plateau (Kirkland et al., 2016b). The Poison Strip Member is a 2- to 15-m-thick stratigraphic package of very fine- to very coarse-grained sandstone and matrix-sup-

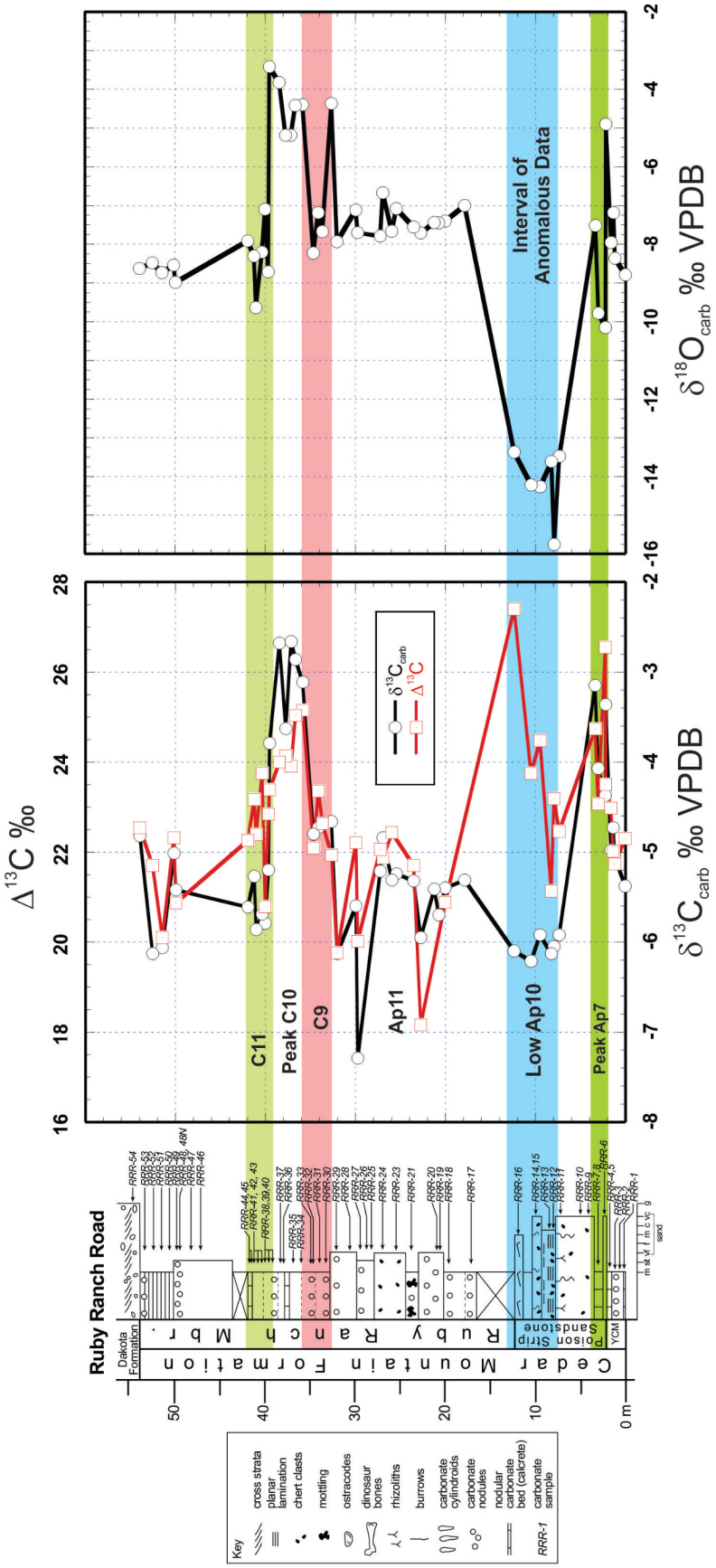

Figure 1. Stable isotope chemostratigraphy of the Cedar Mountain Formation at the Ruby Ranch Road stratigraphic section, Utah (see Fig. 2), modified from Ludvigson et al. (2015). The anomalous whole-rock $\Delta^{13}C$ and carbonate $\delta^{18}O$ values from the Aptian Ap10 interval in the Poison Strip Sandstone Member ("Poison Strip Sandstone" in original figure) of the Cedar Mountain Formation are highlighted in blue. VPDB = Vienna Pee Dee Belemnite.

ported granule to pebble conglomerates with framework grain populations dominated by quartz and having minor feldspar and lithic fragments (Stikes, 2007). The Poison Strip Member is the amalgamated channel-fill and bar deposits of major fluvial systems that flowed northeastward to eastward from the Sevier thrust front and Mogollon Highlands across the Sevier foreland (Jordan 1981; Lawton, 1994; Lawton et al., 2010; Currie, 2002; DeCelles and Coogan, 2006; Stikes, 2007; Dickinson and Gehrels, 2008; Kirkland et al., 2016b). Lacustrine and stromatolitic limestones may be interbedded with, or assume a laterally equivalent position as the fluvial units (Kirkland et al., 2016b). In contrast, both the underlying Yellow Cat and overlying Ruby Ranch Members are dominated by drab to variegated mudrock, which is generally interpreted as floodplain and lacustrine sediments (Kirkland et al., 2016b). The Ruby Ranch Member generally ranges from 15 to 30 m in thickness, although it thickens locally and to the west across the San Rafael Swell, and it is dominated by variegated mudstone and shale with prominent strata of nodular carbonates or "calcretes," for which multiple lines of evidence suggest a palustrine origin (Ludvigson et al., 2010, 2015).

METHODS

This study assesses three samples from the Poison Strip Member in great detail. Two of the specimens come from an outcrop, which is the Ruby

Ranch Road (RRR) locality of Ludvigson et al. (2010, 2015). These samples (RRR-12 and RRR-15) are both medium-grained sandstones. The third sample is a pebble conglomerate from a Utah Geological Survey (UGS) core drilled at Green River, Utah. This core sample is UGS-GRN-184 at the 178-foot-depth level (Figs. 2–3). Several serial cuts were made from this rock sample, and one of them, identified herein as UGS-GRN-184a, was used for stable isotope microsampling. All three rock samples used in this study came from a large research collection directly associated with earlier publications (Ludvigson et al., 2010, 2015). They were selected to address specific questions posed in these prior publications.

Petrographic, diagenetic, stable isotopic, and fluid-inclusion analyses of calcite cements in these samples discriminate the early and late temporal aspects of isotopic variability and crystallization temperatures by establishing the "cement stratigraphy" (Meyers and Lohmann, 1985; Meyers, 1991). Precise petrographic mapping and isotopic microsampling, which avoided inadvertent cross-contamination of cement types, were prerequisites for these analyses.

Petrography

Rock samples were slabbed and vacuum-impregnated with blue-dyed epoxy resins. Epoxy-impregnated slabs were then cut and micropolished. Counterpart micropolished thin (0.03 mm) and thick (1 mm) sections were used for microsampling, following the techniques of Meyers and Lohmann (1985). Petrographic assessments of thin sections were carried out using an Olympus BX51 petrographic microscope with a digital 10.5 megapixel (Mpx) Olympus SC100 color camera. Images were collected under paired plane-polarized and cross-polarized illumination. Epifluorescence images were collected using an Olympus BX53M microscope with a digital 18 Mpx Olympus SC180 color camera. A cathodoluminescence (CL) imaging system allowed for the discrimination of cement types and zonation. A Relion Industries RELIOTRON III cold-cathode chamber—with operating conditions consisting of a rarified helium atmosphere at 50 millitorr, accelerating voltage of 10 kV, and beam current of 0.5 mA—was used for imaging. Macroscale imaging through the 50 mm top window of the chamber was carried out using a 16 Mpx Canon EOS SL1 digital single-lens reflex camera with a macro lens suspended over the CL chamber. Microscale imaging was carried out with the CL chamber mounted on a modified Olympus BX41 compound microscope using a Peltier-cooled 17 Mpx Olympus DP73 color camera. Imaging modes included transmitted light (TL), reflected light (RL), and CL. Macroscale imaging was used to quickly scan 2 × 3 inch and 1 × 2 inch thin and thick sections for the identification of microscopic domains of special interest. Paired microscopic RL and CL images were also collected to map microsampling targets from micropolished thick sections at sub-millimeter scales. All petrographic, fluorescence, and CL imaging was performed at the Kansas Geological Survey.

Intragranular volumes (IGVs) of sandstone samples RRR-12 and RRR-15 were calculated from CL images of luminescent calcite cements to estimate approximate burial depths of cementation using ImageJ, a Java-based image processing program developed at the National Institutes of Health and the University of Wisconsin's Laboratory for Optical and Computational Instrumentation.

Carbonate Microsampling and Stable Isotope Analyses

Carbonate microsampling for stable isotopes was guided by: (1) digital maps of micropolished thick sections acquired with a flatbed scanner; and (2) microscopic RL and CL images that were registered in graphics software to overlap perfectly. A high-precision dental drill with a 0.3 mm-diameter carbide bit was used to extract sample powders (0.05–0.1 mg/sample) from the polished thick sections (Fig. 3). Sample sites were selected and mapped on the matching CL and RL images of polished thick sections in advance to repetitively mill out the calcite components in sub-millimeter space. Thus, we were able to characterize the carbon and oxygen isotopic heterogeneity within each sequential cement zone. Sample powders were roasted in vacuum for 1 hour at 200°C to remove volatile contaminants prior to analysis. The roasted powders were then loaded into single reaction vessels in an automated Kiel III acid-dosing device and reacted with anhydrous phosphoric acid to produce a cryogenically-purified CO_2 gas that was carried to a dual-inlet Thermo Finnigan™ MAT 253 stable isotope mass spectrometer (University of Kansas W.M. Keck-National Science Foundation Paleoenvironmental and Environmental Stable Isotope Laboratory). The subsequent isotopic results were calibrated using the Vienna Pee Dee Belemnite (VPDB) carbonate isotope standard (as in Ludvigson et al., 2015). The uncertainties of the $\delta^{13}C$ and $\delta^{18}O$ measurements are better than ± 0.1‰.

Fluid-Inclusion Analysis

Two doubly polished thick sections (UGS-GRN-184a and UGS-GRN-184b) were prepared from serial cuts of cored rock sample UGS-GRN-184 to enlarge the surface area available for inspection. Our petrographic observations identified both one-phase (liquid) and two-phase (liquid and vapor) fluid inclusions within calcite cements in doubly polished thick sections of the core sample. Consequently, we undertook fluid-inclusion microthermometry measurements using a Linkam THMSG600 stage and a Fluid Flow

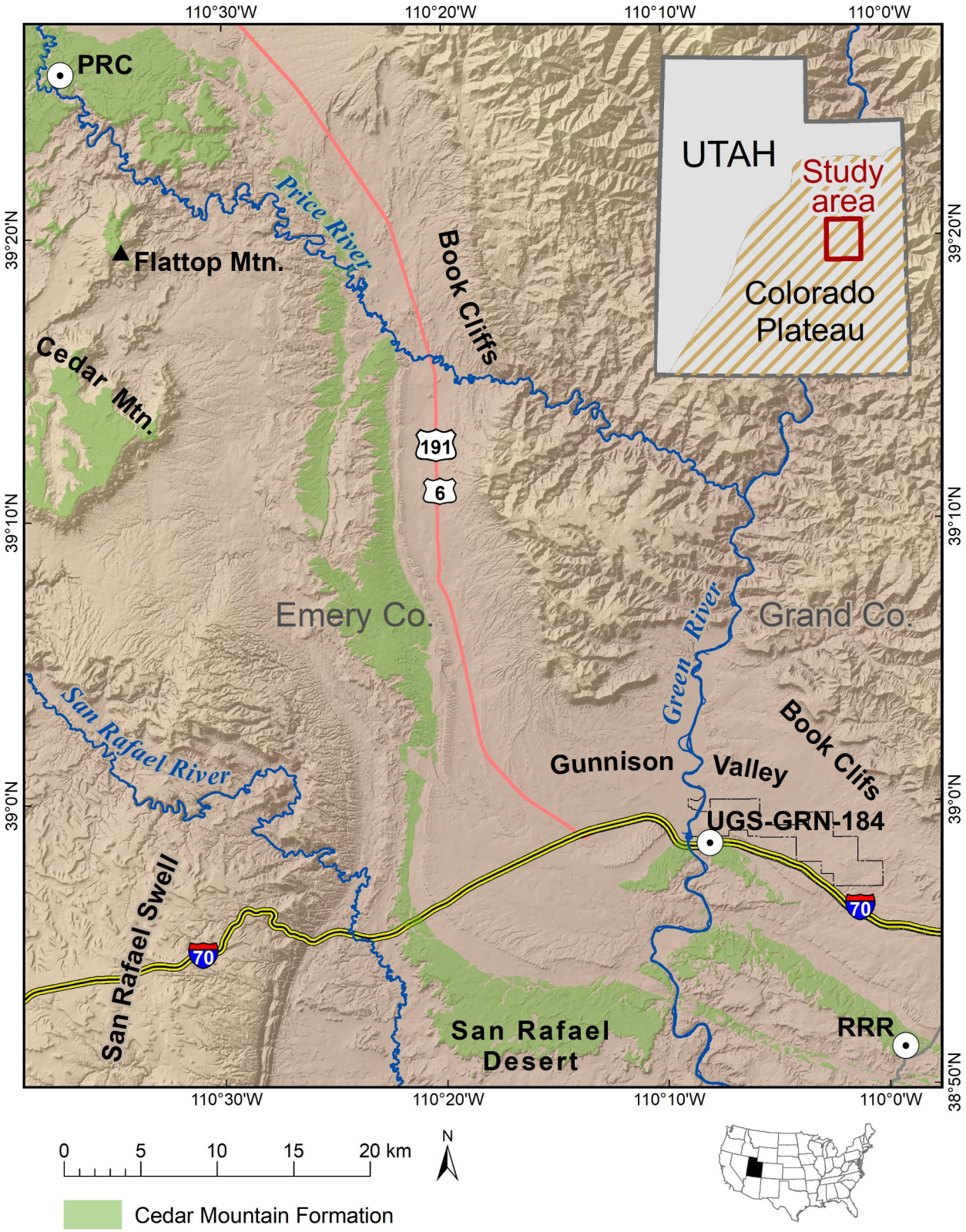

Figure 2. Location map of a portion of eastern Utah, showing the outcrop area of the Cedar Mountain Formation, Ruby Ranch Road (RRR) stratigraphic section, Utah Geological Survey (UGS) GRN-184 core, and Price River (PRC) stratigraphic section.

gas flow heating and cooling system. This system is mounted on an Olympus BX53M infrared microscope that is equipped with 4X, 10X, 40X, and 100X long focal distance objective lenses and with Link Interface Software. Fluid-inclusion micrographs were collected using a 2.7 Mpx FLIR Grasshopper® 3 USB 3.0 digital camera. Samples were examined to ensure full characterization of petrographic associations of fluid inclusions and to establish inclusion origins at the level of fluid-inclusion assemblages (Goldstein and Reynolds, 1994). Salinities are calculated from T_m measurements using equations from Bodnar (1992). Petroleum inclusions were identified using UV epifluorescence and the °API gravity of the oil-bearing inclusions as outlined by Goldstein and Reynolds (1994).

RESULTS

Stratigraphy

Core UGS-GRN-184 includes slightly more than 42 m (138 ft) of the Cedar Mountain Formation (CMF) (Fig. 3). There are no chronostratigraphic data from this core, but the distinct characteristics of three informal stratigraphic intervals within the core (Fig. 3: Intervals I, II, and III) provide a basis for correlations to regional outcrops. Interval I in the core (Fig. 3) is cross-stratified, very fine to medium sandstone and matrix-supported granule to pebble conglomerates. This interval directly overlies the Brushy Basin Member of the Jurassic Morrison Formation. The Yellow Cat Member—which overlies the Morrison Formation to the east of the city of Green River near Arches National Park, and which is overlain by the Poison Strip Member—is absent where the UGS-GRN-184 core was drilled (Kirkland et al., 2016b). Thus, both the stratigraphic position and the lithologic characteristics of Interval I lead us to correlate it as the Poison Strip Member, which is dominated by sandstone and pebbly sandstone (Kirkland, 2016b). Likewise, the variegated mudrock and the seven or eight interspersed nodular carbonate units ("calcretes") comprising the overlying Interval II (Fig. 3) are wholly compatible with the characteristics of the Ruby Ranch Member in outcrops across the enclosing area (Kirkland et al., 2016b). Therefore, we correlate Interval II as a part of the Ruby Ranch Member. Interval III—another sandstone-dominated interval—is also likely to be a part of the Ruby Ranch Member, which contains sandstone bodies in its outcrop belt (Kirkland et al., 1997, 2016b).

Petrography

Samples RRR-12 and RRR-15 are medium-grained sandstone with framework-grain populations dominated by quartz and chert. The optical continuity of 3- to 5-mm-diameter calcite cement crystals in cross-polarized light engulfs the 1- to 2-mm-diameter framework grains, resulting in a poikilotopic fabric. An average intergranular volume of 26.5% was calculated for the sandstone samples of RRR-12 and RRR-15 based on the area filled by the CL luminescent poikilotopic cement in thin-section view (Fig. 4). In addition to the poikilotopic calcite cement, another earlier zone of fine-grained isopachous cement crystals less than 10 microns in width coat the framework grains in samples RRR-12 and RRR-15 (Robertson, 2019). Samples from the Ruby Ranch Road section also contain late-phase, pore-filling bitumen that has undergone shrinkage on rock exposure (Fig. 5).

The poikilotopic cements in RRR-12 and RRR-15 are uniformly luminescent, and lack any variability in CL brightness or color (Figs. 6A–B). Blue-luminescing quartz framework grains, likely of high-temperature origin (Boggs and Krinsley, 2006), as well as a purple-violet luminescent microquartz that overprints the poikilotopic calcite cement, exist in both of the Ruby Ranch Road samples (Figs. 6A–B).

Sample UGS-GRN-184a is a pebble conglomerate near the base of the Poison Strip Member. It has large, sheltered, cm-scale intergranular voids infilled by calcite cements with CL zones of sufficient size (i.e., sampling target-zone diameters that exceed the diameter of the microsampling drill bit) to permit the mapping and microsampling of the full paragenetic sequence of cementation using a 0.3-mm dental burr (Figs. 7A–B). Cement development follows a paragenetic sequence of: (1) calcite cement Zone 1, which is nonluminescent dogtooth isopachous spar 0.5mm to 1 mm in width coating framework grains; (2) nonluminescent chalcedony cement, which replaces calcite cement Zone 1; and (3) calcite cement Zone 2, which is brightly luminescent calcite with equant crystal sizes ranging from 0.1 to 2 mm in size and infills any remaining pore space (Figs. 6C–D). The nonluminescent chalcedony cement preserves ghost structures of dogtooth crystal growth surfaces of calcite cement Zone 1 (Robertson, 2019). Calcite cement Zone 1 is present in all of our samples, but was only developed at a scale of sufficient size to be microsampled in UGS-GRN-184a. This paper seeks to understand the relationship between calcite cement zones 1 and 2 in sample UGS-GRN-184a, and the poikilotopic calcite cements in samples RRR-12 and RRR-15.

Stable Isotope Analyses

A total of 18 carbon and oxygen isotope microsamples were taken from the poikilotopic calcite cements in the micropolished slabs of RRR-12 and RRR-15. Ten microsamples came from calcite cement Zone 1 in the micropolished slab of rock sample UGS-GRN-184a. Seventeen additional microsamples of calcite cement Zone 2 were extracted from the

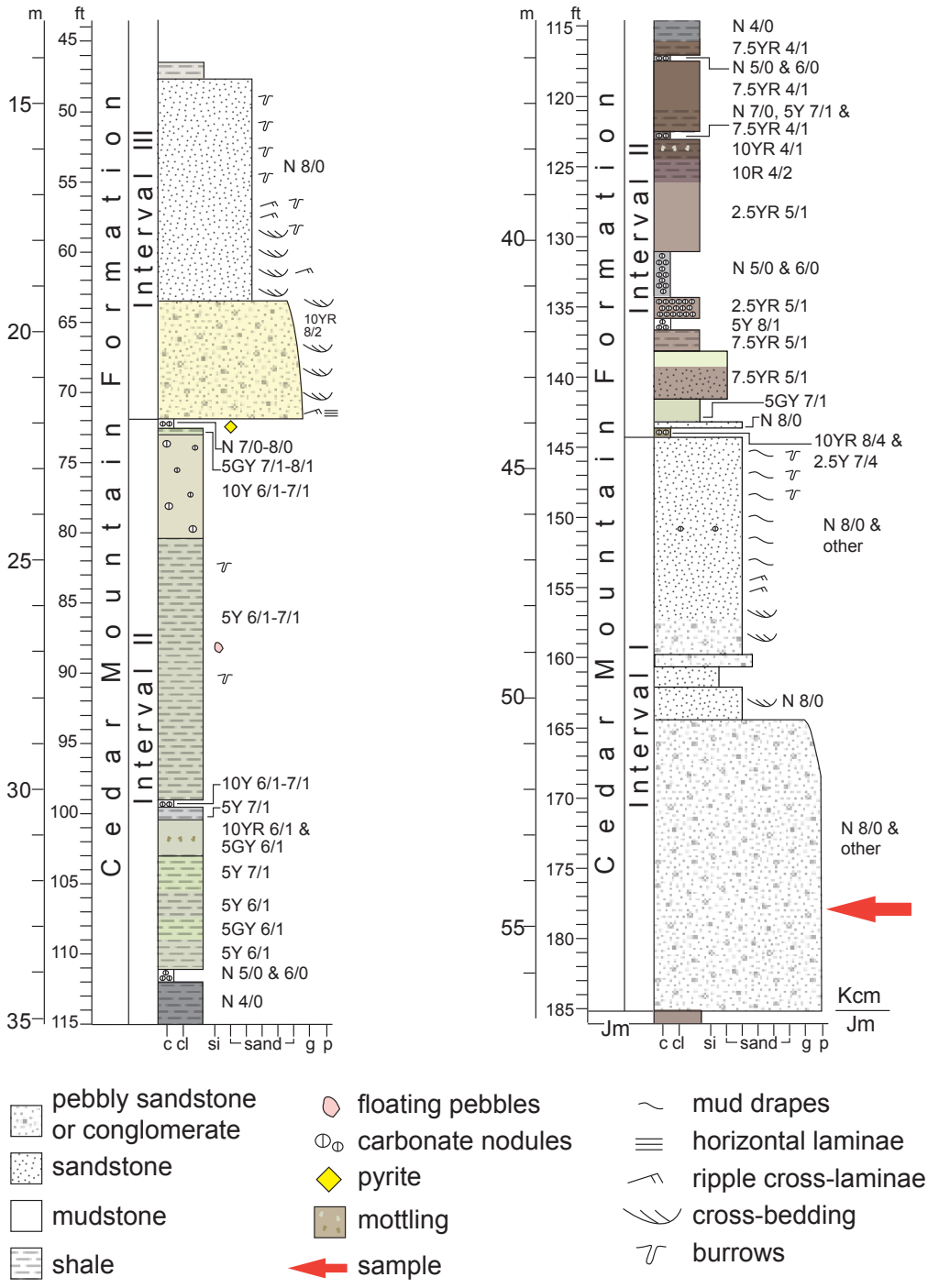

Figure 3. Graphic log of the UGS-GRN-184 core from the vicinity of Green River, Utah. The position of a serially sectioned core sample investigated in this study is shown by the red arrow.

same micropolished slab. Rock samples RRR-12 and RRR-15 yielded similar isotopic results. RRR-12 yielded $\delta^{18}O$ values ranging from -18 to -15‰ VPDB, whereas RRR-15 yielded a slightly narrower range of -17 to -16‰ VPDB. The $\delta^{13}C$ values ranged from -8 to -7‰ VPDB in RRR-12, and -7 to -6 in RRR-15 (Fig. 8). Calcite cements in both sandstone samples yielded relatively invariant carbon and oxygen isotopic compositions in comparison to the total spread of isotopic values (Fig. 8). These values are slightly lower than the oxygen isotopic range of -16 to -13.5‰ VPDB recorded

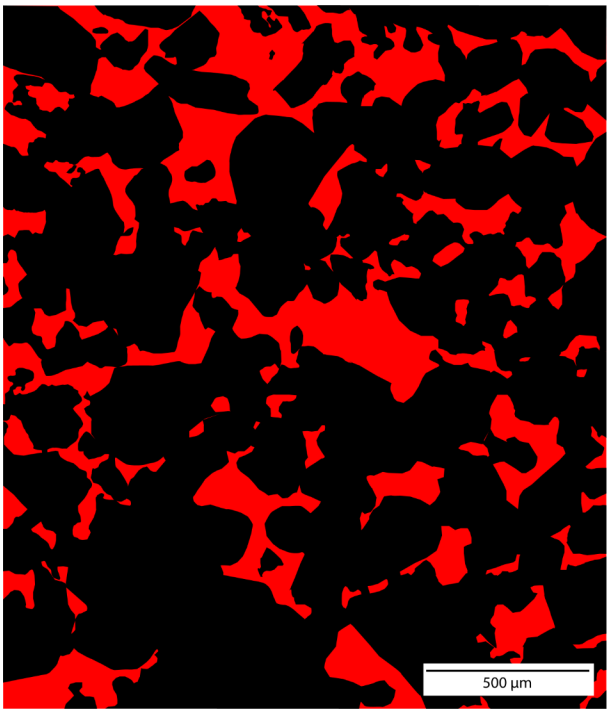

Figure 4. Segmented cathodoluminescence (CL) image (see text for explanation) exhibiting 26% intergranular volume filled by brightly luminescent poikilotopic calcite cement (red) in sample RRR-12, from Robertson (2019). Rigid framework grains appear black.

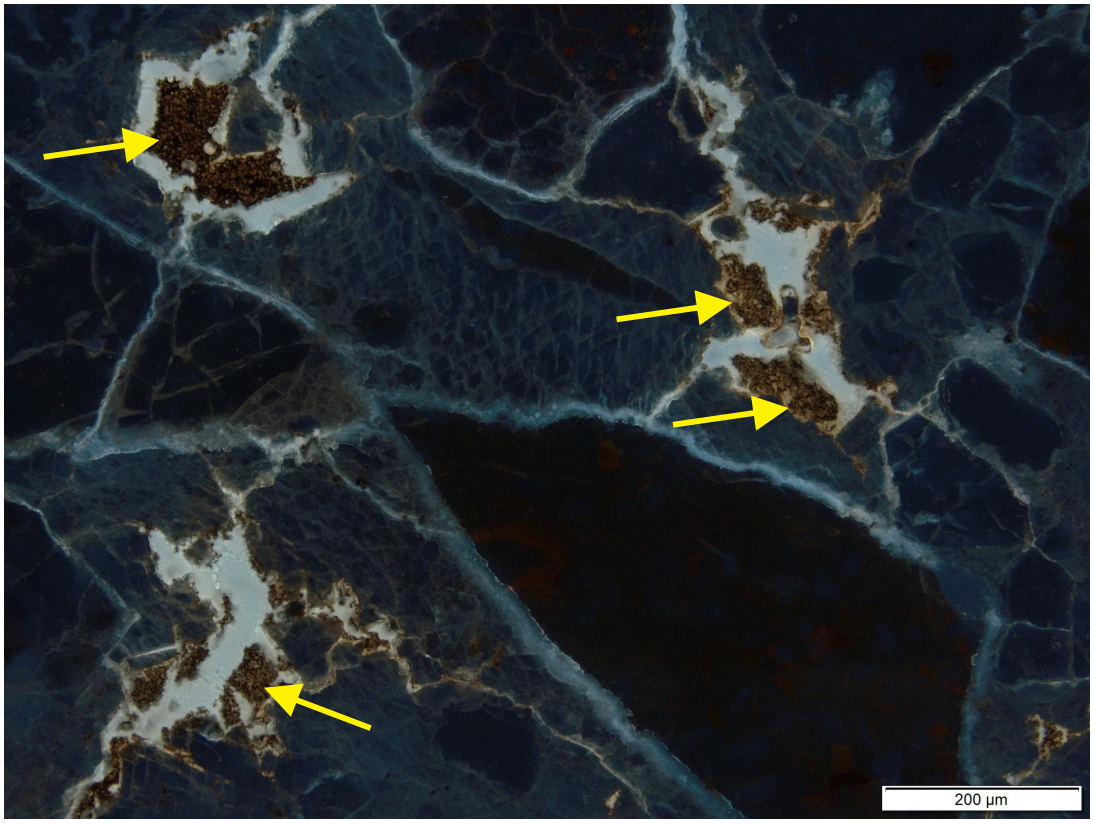

Figure 5. Epifluorescence photomicrograph of bitumen filling pore space remaining after precipitation of luminescent poikilotopic calcite cement in sample RRR-12. White-fluorescing epoxy resin fills open pore space and fractures in the rock. Brown bitumen (yellow arrows) partially fills open pores. Shrinkage of bitumen by loss of volatiles is probably related to the long-term exposure of rock in an arid climate.

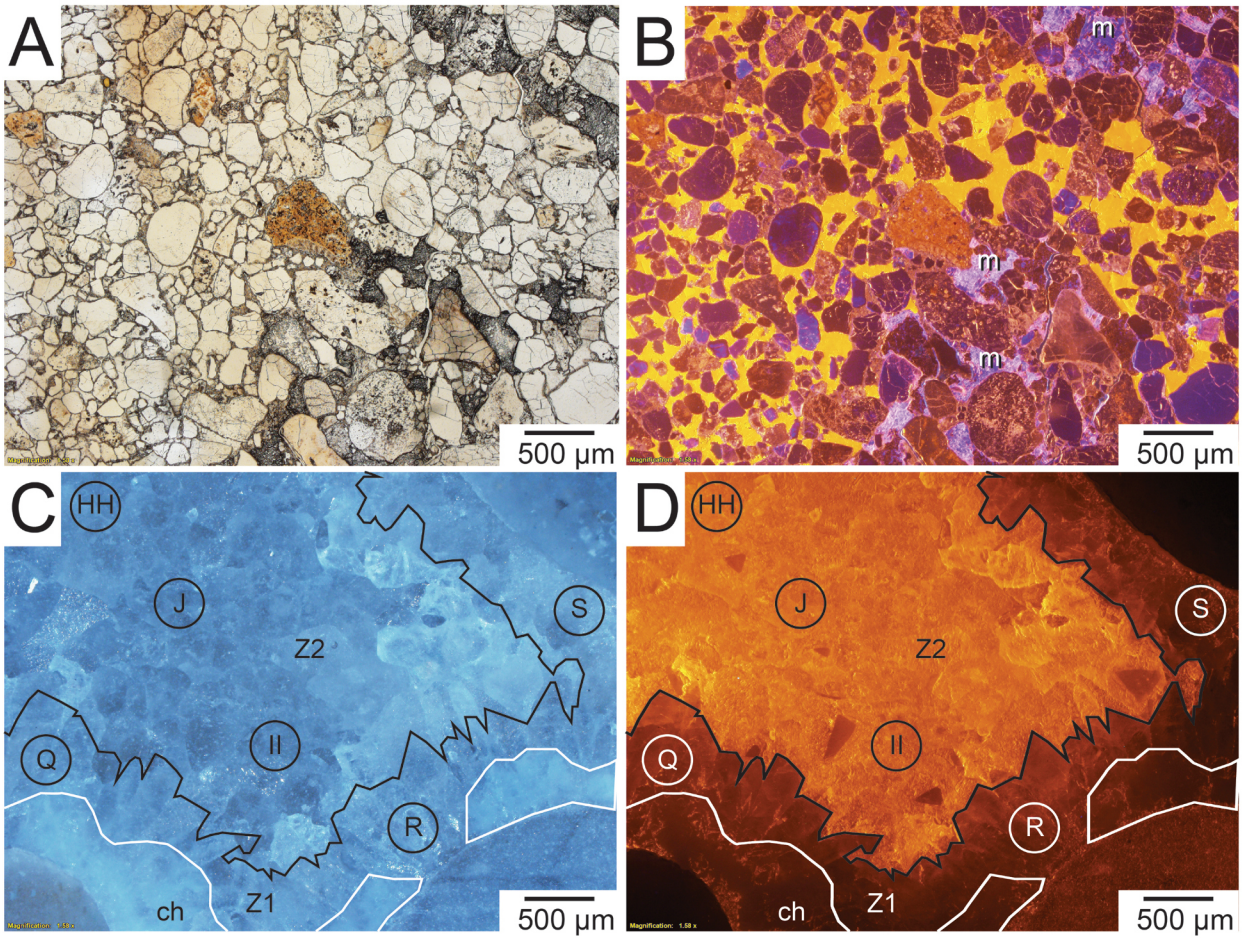

Figure 6. Paired images of transmitted light (TL), reflected light (RL), and CL micrographs of rock samples from the Poison Strip Sandstone Member of the Cedar Mountain Formation, from Robertson (2019). *A*, TL thin-section micrograph of sample RRR-12 showing rock fabric of well-rounded to subangular silicate framework grains. *B*, Same field of view under CL showing bright orange luminescent poikilotopic calcite cement, nonluminescent to dark blue luminescent silicate framework grains, and purple-violet luminescent microquartz (m) overprinting calcite cement. *C*, RL thick-section micrograph of rock sample UGS-GRN-184a showing mapped annotations of the boundaries of calcite cement Zones 1 and 2 (Z1 and Z2, respectively) chosen for microsampling (see text for explanation), as well as nonluminescent chalcedony cement (ch). Circles with letters (HH, II, J, Q, R, S) are microsampling targets for individual carbon and oxygen isotope analyses. Data produced from these microsample sites are archived in Robertson (2019). *D*, CL thick-section micrograph of same field of view from (C) showing the same annotations and microsample sites. Nonluminescent chalcedony has partially replaced calcite cement Zone 1.

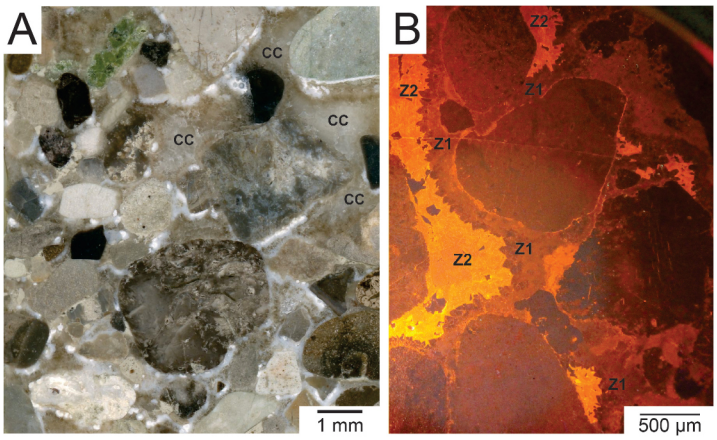

Figure 7. Macroscopic images of the UGS-GRN-184 core. *A*, Scanned RL image of polished core slab showing the positions of calcite cements (CC) filling sheltered voids between silicate framework grains. Note the white, nonluminescent chalcedony cement overprinting fringing calcite cement. *B*, CL image showing nonluminescent calcite cement Zone 1 (Z1) dogtooth calcite and brightly luminescent calcite cement Zone 2 (Z2) filling large, sheltered intergranular voids.

by earlier studies of these same samples using whole-rock analysis (Ludvigson et al., 2015). Calcite cement zones 1 and 2 in the micropolished slab of rock sample UGS-GRN-184a yielded overlapping isotopic values. The initial nonluminescent dogtooth sparry calcite cement of Zone 1 yielded $\delta^{18}O$ values ranging from -10.0 to -8.5‰ VPDB, and $\delta^{13}C$ values ranging from -5.2 to -4.7‰ VPDB (Fig. 8). The pore-filling brightly luminescent sparry calcite of Zone 2 exhibited a wider range of isotopic compositions—$\delta^{18}O$ values ranged from -17.0 to -8.5‰ VPDB, and $\delta^{13}C$ values ranged from -6.5 to -5.0‰ VPDB (Fig. 8).

Fluid-Inclusion Analysis

Petrographic examination of calcite cements in the two doubly polished thick sections of the cored rock sample UGS-GRN-184 (Figs. 2–3) identified fluid inclusions that were the subject of further study. Calcite cements from two serial sections in the core contain one phase (liquid) and two-phase (liquid and vapor) fluid inclusions (Fig. 9). Homogenization temperature (T_h) values range from 86°C to 115°C, and T_m values range from -0.2°C to -0.8°C (Table 1). Petroleum inclusions also were observed in calcite cements with °API gravity ranges estimated from 40 to 45 based on the color of UV fluorescence (Goldstein and Reynolds, 1994) (Figs. 10A–B). Several positive T_m values represent evidence of superheated ice under extreme negative pressure (Adams and Gibson, 1930; Table 1).

DISCUSSION

Cement Paragenesis

The paragenetic sequence of cementation in the Poison Strip Member is readily apparent from petrographic observations of the cement stratigraphy in micropolished thin section and slabs of rock sample UGS-GRN-184a (Fig. 11). The nonluminescent dogtooth calcite of calcite cement Zone 1 is the first phase of cementation, and it coated the largest framework grains in rock sample UGS-GRN-184a. Zone 1 provides the earliest record of diagenetic processes (Figs. 6–7) in the Poison Strip Member. Nonluminescent chalcedony cement precipitated after calcite cement Zone 1 (Fig. 7). This chalcedony cement replaced Zone 1 calcite cement, and it preserves ghost crystal growth structures of that predecessor cement. Brightly luminescent Zone 2 cement fills most of the remaining intergranular volume in the conglomerate, post-dating the earlier calcite cement Zone 1. The brightly luminescent Zone 2 calcite cement in micropolished thin sections and slabs of rock sample UGS-GRN-184a partially overprints the nonluminescent chalcedony and calcite cement Zone 1 calcite as a later pore-filling phase, providing further evidence for its relatively younger age and its placement in the paragenetic sequence (Fig. 7).

The poikilotopic calcite cements in the RRR-12 and RRR-15 samples fill intergranular volumes that range from 23.5% to 26.5%. Intergranular volumes in medium-grained sandstones in that range are characteristic of cementation of rigid-grained sandstones after pore space has collapsed under lithostatic loading at deep burial conditions of 2 to 3 km (Paxton et al., 2002, their fig. 6).

Pore-filling bitumen (Fig. 5) is an irrefutable indicator that petroleum migrated through the Poison Strip Member during a late stage of diagenesis. This petroleum migration filled pore space remaining after the preceding stages of cementation, and terminated the precipitation of poikilotopic calcite cements in RRR-12 and RRR-15. We hypothesize that pore space that now exists between any remaining bitumen and the surrounding calcite cement resulted from volume reduction as organic volatiles were lost with exposure at Earth's surface (Fig. 5). The origin and age of the bright purple-violet luminescent microquartz cements in RRR-12 and RRR-15 remain unclear. These silica cements overprint the brightly luminescent poikilotopic calcite cements, placing them at later stage in the paragenetic sequence (Figs. 6A–B). Furthermore, CL properties of the bright violet-colored silica cement are unlike those of the nonluminescent chalcedony cements observed in thin sections from rock sample UGS-GRN-184a. Therefore, the two silica cements from two different locations probably are not genetically related.

Diagenetic Analysis of Strata from the Early Aptian Ap10 Interval

The early Aptian Ap10 interval was defined by Herrle et al. (2004) from high-resolution chemostratigraphic profiles of Cretaceous C-isotope stratigraphy. It is characterized by a pronounced minimum in $\delta^{13}C$ values occurring between higher $\delta^{13}C$ values of the early Aptian Ap7 and the late Aptian Ap15 intervals of Herrle et al. (2004). Ludvigson et al. (2010, 2015) correlated chemostratigraphic profiles of the Ap10 interval between the Ruby Ranch Road (RRR) and the Price River (PRC) stratigraphic sections (Fig. 2). From the Price River stratigraphic section (Ludvigson et al., 2010, 2015), rock sample PRC-23 from the Ap10 interval correlates with RRR-12 and RRR-15 from the Ruby Ranch Road stratigraphic section. Diagenetic evaluations of carbon-oxygen isotope data from the RRR rock samples, along with the correlative interval in the UGS-GRN-184 core, provide the basis for interpreting the early-to-late diagenetic evolution of strata from the Ap10 interval in the Cretaceous foreland basin. The special utility of this cored conglomerate sample at Green River, Utah, is that the large sheltered intergranular voids filled by calcite

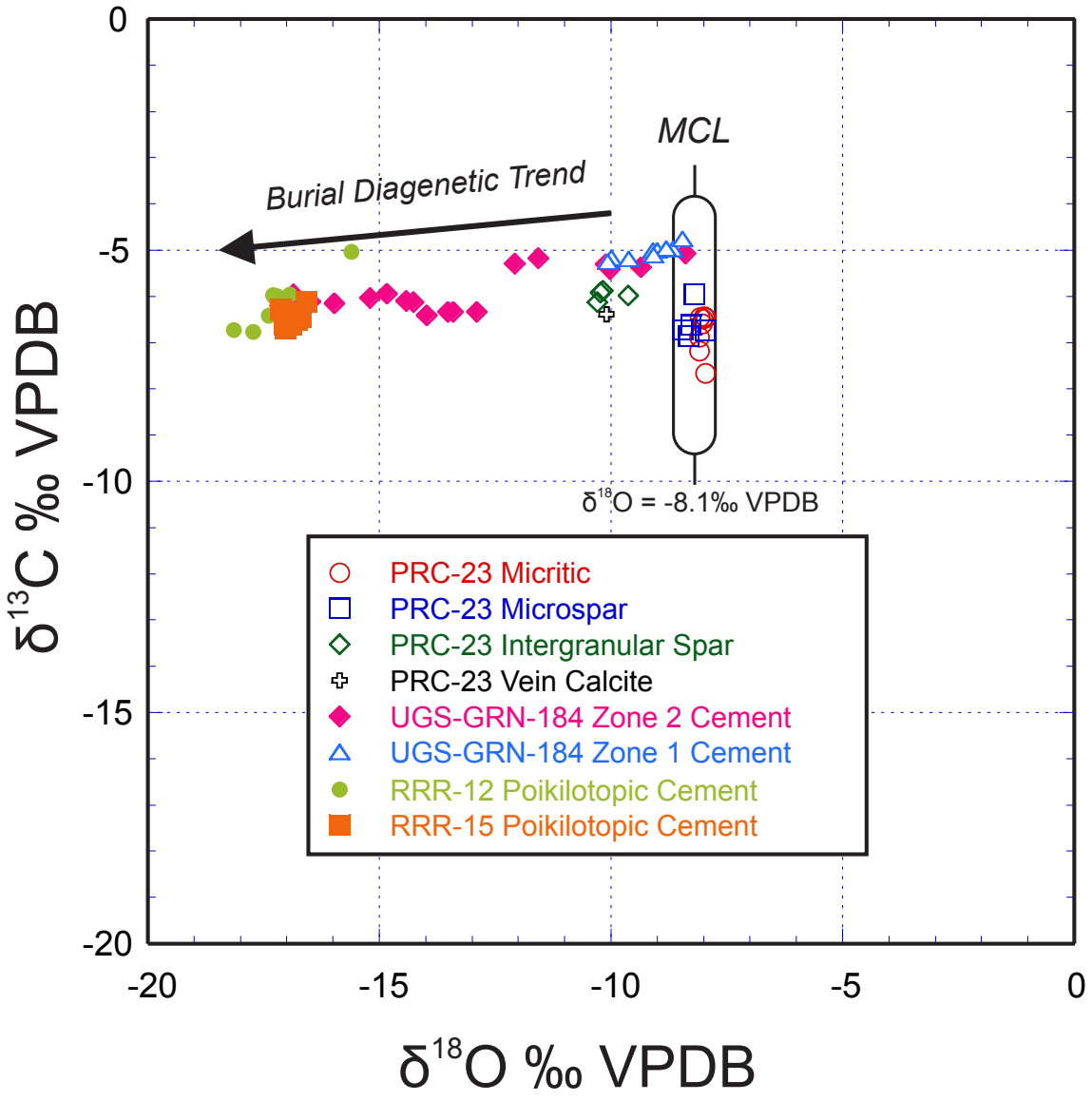

Figure 8. Carbon-oxygen isotope plot of diagenetic carbonate components from the Ap10 interval of the Cretaceous Cedar Mountain Formation. The meteoric calcite line (MCL) trend from rock sample PRC-23 of $\delta^{18}O$ = -8.1 ± 0.16‰ VPDB was discussed earlier by Ludvigson et al. (2010, 2015). The burial diagenetic trend from poikilotopic calcite cements in rock samples RRR-12 and RRR-15, and calcite cements in UGS-GRN-184 core depicts newly produced data from strata of the Poison Strip Sandstone Member from this study.

cements preserve CL-mapped zones of sufficient thickness to define and microsample the cement stratigraphy (Meyers, 1991). This approach permits the interpretation of the mineral paragenesis and diagenetic history of the Ap10 interval (Fig. 7).

Ludvigson et al. (2010) presented a diagenetic evaluation of rock sample PRC-23 from the chemostratigraphic profile of the Price River stratigraphic section, contrasting results from both the authigenic micritic or microspar components as well as later diagenetic vein or intergranular spar components. By combining these data (Ludvigson et al., 2010) with results from stratigraphically equivalent rock samples from the Poison Strip Member at Ruby Ranch Road (RRR-12 and RRR-15) and the UGS-GRN-184 core (Fig. 8), we can clearly define carbon-oxygen isotope values that are characteristic of early meteoric diagenesis, enabling the discrimination of products of early from later burial diagenesis in the CMF.

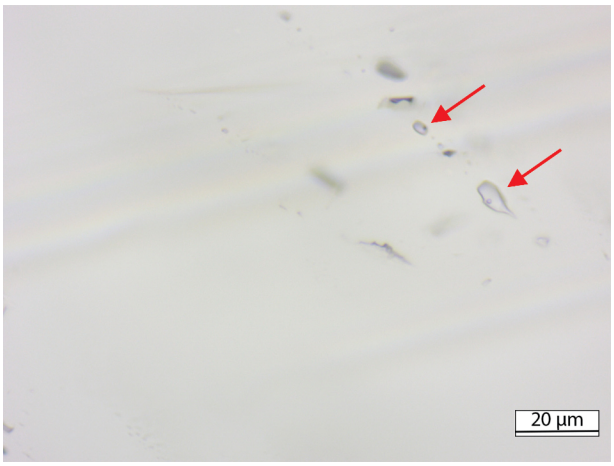

Figure 9. Photomicrograph of fluid inclusions in calcite cement from the UGS-GRN-184 core. Assemblage of pseudo-secondary single-phase and two-phase inclusions in open-space-filling calcite cement.

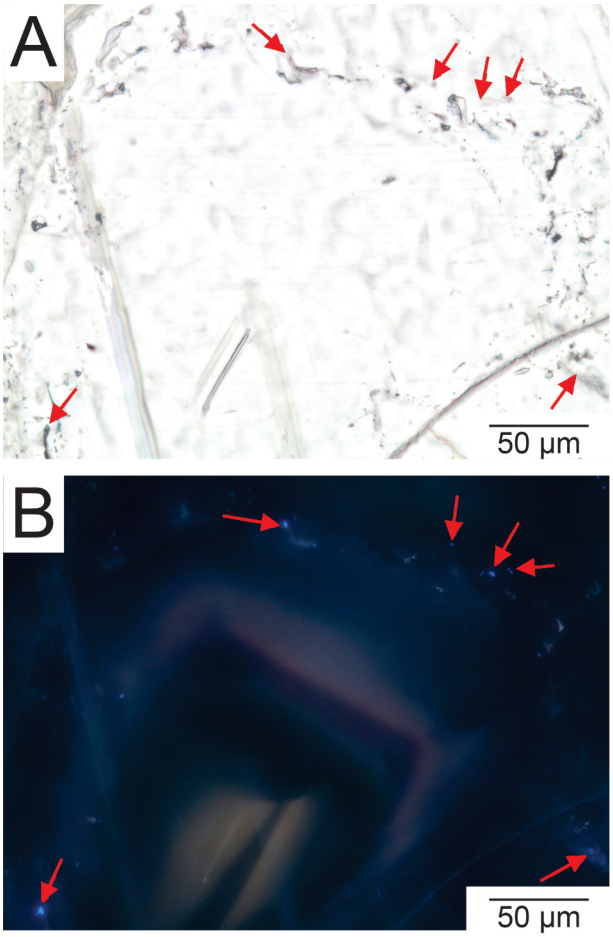

Figure 10. Fluid-inclusion photomicrographs taken from calcite cements in the UGS-GRN-184 core. *A*, Transmitted-light image of assemblage of secondary petroleum-bearing inclusions (red arrows) in calcite cement. *B*, Ultraviolet fluorescence image from the same field of view, showing light blue fluorescence of petroleum-bearing inclusions (red arrows). Note epifluorescent crystal growth zonation in calcite cement.

Diagenetic Interpretations of Carbonate Component Stable Isotope Data

Interpretations of the carbon and oxygen isotope data from calcite cements in the Poison Strip Member are based on recognition of distinctive patterns in carbon and oxygen isotope space that are characteristic of individual carbonate components, and on the well-documented scientific literature on interpretations of carbonate diagenesis. Burial cements typically have highly variable $\delta^{18}O$ values and comparatively invariant $\delta^{13}C$ values (Choquette and James, 1987). This covariant isotope pattern is primarily the result of increasing temperatures of precipitating waters under burial conditions, and the retrograde solubility of calcite (Choquette and James, 1987; Algeo et al., 1992; Hasiuk et al., 2016). A markedly different covariant spatial pattern is characteristic of early meteoric diagenesis, where a vertical trend of highly variable $\delta^{13}C$ values with relatively invariant $\delta^{18}O$ values, known as the "meteoric calcite line" (Choquette and James, 1987; Lohmann, 1988; Hasiuk et al., 2016). The carbon and oxygen isotope pattern observed in burial diagenetic environments was verified by Hasiuk et al. (2016) in a study that examined 28 subsurface petroleum reservoirs. The carbonate isotopic data taken from the Poison Strip Member clearly displays highly variable $\delta^{18}O$ values with a covariant carbon and oxygen isotope linear trend with positive slope, matching the signature typically associated with carbonates influenced by burial diagenetic environments (Fig. 8).

Calcite cement Zone 1—the first phase of pore-filling cement and the earliest record of diagenesis—contains the highest $\delta^{18}O$ values (-10.0 to -8.5‰ VPDB). The pattern of carbon and oxygen isotopic variation in Zone 1 calcite converges with the meteoric calcite line documented from correlative rock sample PRC-23 (Ludvigson et al., 2010), suggesting origin from early meteoric diagenesis during initial lithification of the conglomerate. This range of $\delta^{18}O$ values is also similar to the $\delta^{18}O$ values identified from burial diagenetic cements and those from authigenic components of rock sample PRC-23 from the Ap10 interval at the Price River stratigraphic section (Ludvigson et al., 2010, 2015). Petrographic observations indicate that the brightly luminescent calcite cement of Zone 2 partly replaces the nonluminescent Zone 1 cement, and while this intimate relationship provides cogent evidence for a paragenetic relationship, it also poses a challenge for the isolation of cement zones during microsampling. Thus, our ambiguous $\delta^{18}O$ values from calcite cement Zone 1 may possibly reflect in-

Table 1. Microthermometric data for fluid inclusions in calcite cements in rock sample UGS-GRN-184 core (Th = homogenization temperature; Tm = last ice-melting temperature).

Sample ID	Host Mineral	Assemblage	T_h (°C)	T_m (°C)	Calculated salinity (wt% eq. NaCl)	Comments
UGS-GRN-184a	Calcite	Assemblage 1	90.5	+0.6	-	Pseudo-secondary, super-heated ice under extreme negative pressure
			90.5	-	-	Pseudo-secondary
			100	-	-	
			90.3	-0.2	0.4	
			87			
			97	-0.2	0.4	
			97	+1.6	-	Pseudo-secondary – super-heated ice under extreme negative pressure
UGS-GRN-184b	Calcite	Assemblage 1	100	+1.1	-	Secondary- super-heated ice under extreme negative pressure
			86.5	-	-	
			100	+0.9	-	
			100	+0.9	-	
			100	+0.5	-	Secondary- super-heated ice under extreme negative pressure
		Assemblage 2	115	-0.8	1.4	Secondary
			115	-0.8	1.4	
			115	-0.8	1.4	
			115	-0.8	1.4	
			115	-0.8	1.4	
			115	-0.8	1.4	
			115	-0.8	1.4	
			115	-0.8	1.4	
			115	-0.8	1.4	
			115	-0.8	1.4	
			115	-0.8	1.4	
			115	-0.8	1.4	
			115	-0.8	1.4	
			115	-0.8	1.4	
			115	-0.8	1.4	
			115	-0.8	1.4	

advertent solid-phase mixing with material from calcite cement Zone 2 during sample extraction (Fig. 8). Although it remains a possibility that Zone 1 is solely an early meteoric diagenetic cement, the overall pattern of the data in carbon and oxygen isotope space could also suggest that Zone 1 may preserve a record of the earliest stages of burial-diagenetic cementation.

Calcite cement Zone 2 yielded $\delta^{18}O$ values ranging from -17.0 to -8.5‰ VPDB. These values plot in the gap between the higher Zone 1 $\delta^{18}O$ values and the much lower $\delta^{18}O$ values observed in the poikilotopic calcite cements samples from RRR-12 and RRR-15 (Fig. 8). The comparatively large oxygen isotopic variation in this cement zone suggests precipitation over a longer time span with chang-

ing subsurface temperatures relative to the other calcite cements sampled from the Cretaceous Ap10 interval (Hasiuk et al., 2016).

Poikilotopic calcite cements in samples RRR-12 and RRR-15 yielded the lowest $\delta^{18}O$ values of any components sampled from the CMF (Fig. 8). Therefore, we consider them to be responsible for the anomalously low $\delta^{18}O$ values originally generated by whole-rock isotopic analysis of the Poison Strip Member (Fig. 1). The stable isotopic data obtained from microsamples of rock sample UGS-GRN-184a clarified the relative timing and diagenetic environments of the poikilotopic cements microsampled from slabs of the Ruby Ranch Road rock samples. The poikilotopic calcite cements from the Ruby Ranch Road section and the Zone 2 cements from micropolished slabs of the UGS-GRN-184a rock sample have overlapping stable isotope compositions and similar crystal morphologies and CL luminescence characteristics. They represent the same stage of burial diagenesis. Poikilotopic calcite cements represent a later stage of pore-filling in the paragenetic sequence of the Poison Strip Member, the only later stages being bitumen pore fills and violet-luminescent microquartz cement (Fig. 11).

Burial Depth and Temperature

The average intergranular volume of 26.5% filled by the poikilotopic cements of samples RRR-12 and RRR-15 (Fig. 6) indicates burial depths ranging from 2 to 3 km (Paxton et al., 2002). This estimate is logically consistent with the thickness of overlying Cretaceous and Cenozoic strata eroded from the adjacent Book Cliffs (Fisher et al., 1960). Applying geothermal gradients ranging between 25° and 45°C per km of depth (Blackett and Wakefield, 2004) to this proposed depth range estimates burial temperatures of 75° to 155°C during the precipitation of the poikilotopic calcites cements. This estimate overlaps with the fluid-inclusion filling temperatures ranging from 87°C to 115°C from the calcite cements in rock sample UGS-GRN-184a.

In order to contrast early depositional from later burial temperatures, the temperatures of early meteoric diagenesis during the deposition of the Poison Strip Member can be estimated through the method described by Suarez et al. (2009). This method employs a second-order polynomial regression (Ufnar et al., 2002; Suarez et al., 2009), based on a Cretaceous latitudinal temperature gradient (Spicer and Corfield, 1992) that was calculated on the basis of fossil-leaf physiognomy (Wolfe and Upchurch, 1987). The equation of Suarez et al. (2009) is:

$$t = 30.25 - 0.2025l - 0.0006l^2$$

where t is temperature (°C), and l is paleolatitude. Using a paleolatitude of 34°N specified for the CMF, the Suarez et al. (2009) equation results in a calculated mean annual depositional surface temperature of 23.4°C. This mean annual temperature is also an estimate of the shallow subsurface temperatures of the meteoric waters from which calcite crystallization took place during early diagenesis, be-

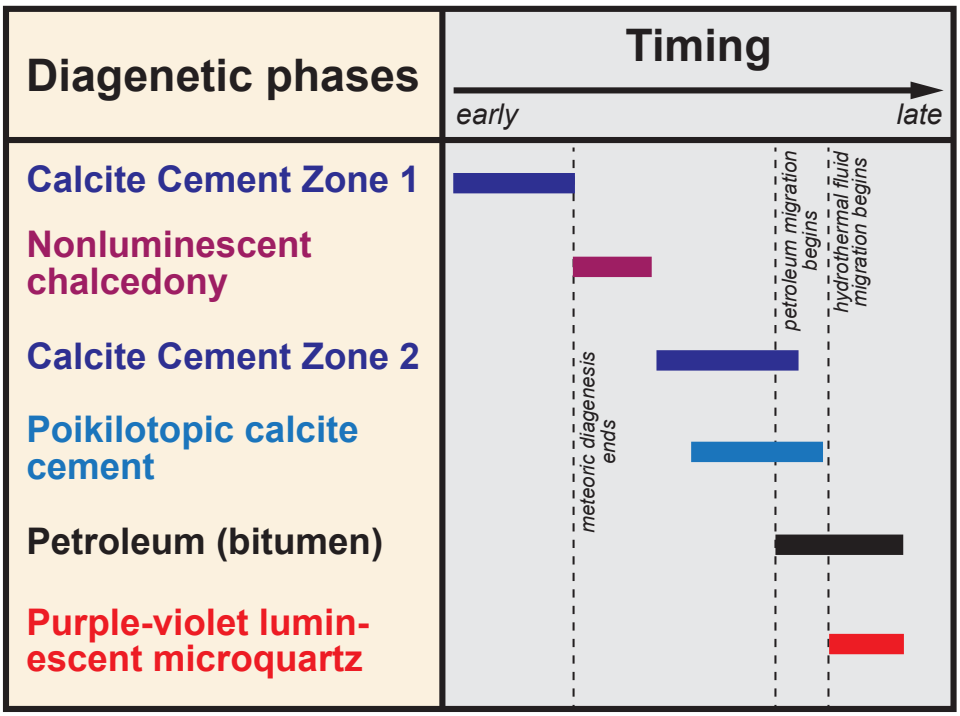

Figure 11. Mineral paragenesis of diagenetic products in the Poison Strip Sandstone Member (modified after Robertson, 2019).

cause shallow groundwater usually takes on the mean annual temperature of a location (Lohmann, 1988).

Influence of Petroleum Migration

Pore-filling bitumen (Fig. 5), a late paragenetic stage (Fig. 11), indicates basinal petroleum migration. This observation is unsurprising, because the Cedar Mountain and correlative Burro Canyon Formations are important oil and natural gas reservoirs in the Paradox Basin (Whidden et al., 2014, their fig. 13). This study presents the first published petrographic evidence for the migration of petroleum and other fluids through the Poison Strip Member. It is possible that petroleum migration occurred after or coincided with the precipitation of poikilotopic calcite cements. We originally estimated burial temperatures of 75° to 155°C, and measured fluid-inclusion filling temperatures ranging from 86° to 115°C. These temperature ranges would place the Poison Strip Member within the oil generation window during the growth of the poikilotopic calcite cement (Eremenko and Tverdova, 1980). Therefore, it is plausible that the fluids associated with petroleum migration influenced the precipitation of the poikilotopic calcite cements, and that they were also responsible for the low $\delta^{18}O$ values derived from the unit. The burial diagenetic pattern of carbonates with widely ranging $\delta^{18}O$ values that are arrayed along linear trends with positive slopes in carbon-oxygen isotope space, as documented in this work, is a characteristic of ancient carbonates influenced by petroleum migration (Hasiuk et al., 2016; Ross et al., 2020).

The timing and origin of the purple-violet CL luminescent silica cements (Figs. 6A–B) are unknown. The color of these cements, however, is compatible with an origin as quartz polymorphs that crystallized from hydrothermal solutions (Götze and Zimmerle, 2000; Götze et al., 2001; Witke et al., 2004; Boggs and Krinsley, 2006). Thus, we speculate that purple-violet luminescent silica cements crystallized from hydrothermal fluids emanating from the La Sal Mountains, Oligocene laccolith remnants some 40 km distant that are part of a larger regional trend of igneous activity and that exhibit common evidence for hydrothermal alteration, including the crystallization of silica (Hunt, 1958; Nelson et al., 1992; Ross, 1998).

Fluid Inclusions

A fluid-inclusion study of the calcite cement in this investigation indicates T_h values ranging from 86° to 115°C, compatible with but below the maximum burial temperatures estimated from intergranular volumes preserved in rock samples RRR-12 and RRR-15. The distribution of fluid inclusion results along with carbon and oxygen isotope data indicate that these fluids (secondary and pseudo-secondary inclusions) are associated with migration of inter-strata water and petroleum during later stages of diagenesis. These oil-bearing inclusions with light blue color in epifluorescence light indicate intense ultraviolet with higher °API gravity. These oil-filled inclusions seem to be filled with immature to mature petroleum that migrated in the later stage of diagenesis. This migration is most likely associated with the petroleum system in the Paradox Basin (Whidden et al., 2014).

These data further support the idea that the anomalous lower carbonate $\delta^{18}O$ values associated with the Poison Strip Member of the CMF are not associated with low-temperature meteoric calcite line patterns in carbon-oxygen isotope space, but rather with an isotopic pattern associated with higher temperatures during burial diagenesis. Accordingly, the low whole-rock $\delta^{18}O$ values are not products of early meteoric diagenesis, and the idea of an authigenic record of a Cretaceous paleoclimatic event in the Poison Strip Member is not supported. Likewise, the anomalous whole-rock $\Delta^{13}C$ values reported from the Poison Strip Member are not the result of any possible entrainment of sedimentary organic carbon particles from Cretaceous alpine paleofloras, but rather the presence of pore-filling bitumen that resulted from petroleum migration in the unit under burial conditions.

CONCLUSIONS

The low $\delta^{18}O$ values of whole-rock carbonate cements in the Poison Strip Sandstone Member, atypical of the Cedar Mountain Formation (CMF), are not representative of authigenic processes in the CMF, but rather are the result of deeper burial diagenesis. The precipitation of late-stage poikilotopic calcite cements in the Poison Strip Member was likely associated with petroleum migration in the Paradox Basin. Nearby Oligocene laccolith emplacement in the La Sal Mountains might have also played an additional role by providing hydrothermal fluids for late silica cementation. Additional geochemical studies are needed to further explore the burial and thermal evolution of the petroleum system in the Paradox Basin. Our results clearly show that sandstone of the Poison Strip Member served as preferential flow paths for higher-temperature fluids, processes that resulted in anomalous whole-rock isotopic values in the CMF.

ACKNOWLEDGMENTS

Co-author James Kirkland thanks the late Richard Dayvault (U.S. Department of Energy) for securing the UGS-GRN-184 core for the Utah Geological Survey Core Repository. We thank Bruce Barnett at the University of Kansas W.M. Keck-National Science Foundation Paleoenvironmental and Environmental Stable Isotope Laboratory for supervision of the stable isotope analyses carried out for

this work. We thank our Kansas Geological Survey colleague Franciszek 'Franek' Hasiuk for technical review of an earlier draft, and Utah Geological Survey colleagues Donald DeBlieux, Grant Willis, and Stephanie Carney for technical reviews. We thank peer reviewers B. Ronald Frost, Laura Crossey, Sally Potter-McIntyre, and Minyu Yang for helpful suggestions that improved our presentation. Appreciation is extended to *Rocky Mountain Geology* Managing Editor Brendon Orr for editorial assistance.

REFERENCES CITED

Adams, L.H., and Gibson, R.E., 1930, The melting curve of sodium chloride dihydrate. An experimental study of an incongruent melting at pressures up to twelve thousand atmospheres: Journal of the American Chemical Society, v. 52, p. 4,252–4,264.

Algeo, T.J., Wilkinson, B.H., and Lohmann, K.C., 1992, Meteoric-burial diagenesis of Middle Pennsylvanian limestones in the Orogrande Basin, New Mexico: Water/rock interactions and basin geothermics: Journal of Sedimentary Petrology, v. 62, p. 652–670.

Blackett, R.E., and Wakefield, S.I., 2004, Geothermal resources of Utah: A digital atlas of Utah's geothermal resources: Utah Geological Survey Open-File Report 397, 95 p.

Bodnar, R.J., 1992, The system H_2O-NaCl (Abstract): PACROFI IV, Fourth Biennial Pan-American Conference on Research on Fluid Inclusions, Lake Arrowhead, California, Program and Abstracts, v. 4, p. 108–111.

Boggs, S., and Krinsley, D., 2006, Application of cathodoluminescence imaging to the study of sedimentary rocks: New York, New York, Cambridge University Press, *x* +176 p.

Choquette, P.W., and James, N.P., 1987, Diagenesis #12: Diagenesis in limestones – 3: The deep burial environment: Geoscience Canada, v. 14, p. 3–5.

Currie, B.S., 2002, Structural configuration of the Early Cretaceous Cordilleran foreland-basin system and Sevier thrust belt, Utah and Colorado: Journal of Geology, v. 110, p. 697–718.

DeCelles, P.G., and Coogan, J.C., 2006, Regional structure and kinematic history of the Sevier fold-thrust belt, central Utah: Implications for the Cordilleran magmatic arc and foreland basin system: Geological Society of America Bulletin, v. 118, p. 841–864.

Dettman, D.L., and Lohmann, K.C., 2000, Oxygen isotope evidence for high-altitude snow in the Laramide Rocky Mountains of North America during the Late Cretaceous and Paleogene: Geology, v. 28, p. 243–246.

Dickinson, W.R., and Gehrels, G.E., 2008, Sediment delivery to the Cordilleran foreland basin: Insights from U-Pb ages of detrital zircons in Upper Jurassic and Cretaceous strata of the Colorado Plateau: American Journal of Science, v. 308, p. 1,041–1,082.

Edwards, T.W.D., Graf, W., Trimborn, P., and three others, 2000, $\delta^{13}C$ response surface resolves humidity and temperature signals in trees: Geochimica et Cosmochimica Avta [Geochemistry and Cosmochemistry Transactions], v. 64, p. 161–167.

Ehleringer, J.R., and Monson, R.K., 1993, Evolutionary and ecological aspects of photosynthetic pathway variation: Annual Review of Ecology, Evolution, and Systematics, v. 24, p. 411–439.

Eremenko, N.A., and Tverdova, R.A., 1980, Sorbed hydrocarbons in dispersed organic matter: Geology of Oil and Gas, v. 12, p. 26–31.

Fisher, D.J., Erdmann, C.E., and Reeside, J.B., Jr., 1960, Cretaceous and Tertiary formations of the Book Cliffs, Carbon, Emery, and Grand counties, Utah, and Garfield and Mesa counties, Colorado: U.S. Geological Survey Professional Paper 332, *iv* + 80 p.

Glancy, T.J., Jr., Arthur, M.A., Barron, E.J., and Kauffman, E.G., 1993, A paleoclimate model for the North American Cretaceous (Cenomanian-Turonian) epicontinental sea, *in* Caldwell, W.G.E., and Kauffman, E.G., eds., Evolution of the Western Interior Basin: St. John's, Newfoundland, Canada, Geological Association of Canada Special Paper 39, p. 219–241.

Goldstein, R.H., and Reynolds, T.J., 1994, Systematics of fluid inclusions in diagenetic minerals: Tulsa, Oklahoma, Society for Sedimentary Geology Short Course 31, *xii* + 199 p.

Götze, J., and Zimmerle, W., 2000, Quartz and silica as guide to provenance in sediments and sedimentary rocks: Contributions to Sedimentary Geology, v. 21, *iv* + 91 p.

Götze, J., Plötze, M., and Habermann, D., 2001, Origin, spectral characteristics and practical applications of the cathodoluminescence (CL) of quartz – a review: Mineralogy and Petrology, v. 71, p. 225–250.

Hasiuk, F.J., Kaczmarek, S.E., and Fullmer, S.M., 2016, Diagenetic origins of the calcite microcrystals that host microporosity in limestone reservoirs: Journal of Sedimentary Research, v. 86, p. 1,163–1,178.

Herrle, J.O., Kößler, P., Oliver, F., and two others, 2004, High-resolution carbon isotope records of the Aptian to Lower Albian from SE France and the Mazagan Plateau (DSDP Site 545): A stratigraphic tool for paleoceanographic and paleobiologic reconstruction: Earth and Planetary Science Letters, v. 218, p. 149–161.

Hunt, C.B., 1958, Structural and igneous geology of the La Sal Mountains, Utah: U.S. Geological Survey Professional Paper 294–I, p. 305–364.

Joeckel, R.M., Ludvigson, G.A., and Kirkland, J.I., 2017, Lower Cretaceous paleo-Vertisols and sedimentary interrelationships in stacked alluvial sequences, Utah, USA: Sedimentary Geology, v. 361, p. 1–24.

Joeckel, R.M., Ludvigson, G.A., Möller, A., and six others, 2019, Chronostratigraphy and terrestrial palaeoclimatol-

ogy of Berriasian–Hauterivian strata of the Cedar Mountain Formation, Utah, USA, *in* Wagreich, M., Hart, M.B., Sames, B., and Yilmaz, I.O., eds., Cretaceous climate events and short-term sea-level changes: London, United Kingdom, Geological Society of London Special Publication 498, p. 75–100, https://doi.org/10.1144/SP498-2018-133.

Jordan, T.E., 1981, Thrust loads and foreland basin evolution, Cretaceous, Western United States: American Association of Petroleum Geologists Bulletin, v. 65, p. 2,506–2,520.

Kirkland, J.I., Britt, B.B., Burge, D.L., and six others, 1997, Lower to Middle Cretaceous dinosaur faunas of the central Colorado Plateau: A key to understanding 35 million years of tectonics, sedimentology, evolution and biogeography: Brigham Young University Geology Studies 42, p. 69–103.

Kirkland, J.I., Simpson, E.L., DeBlieux, D.D., and three others, 2016a, Depositional constraints on the Lower Cretaceous Stikes Quarry dinosaur site: Upper Yellow Cat Member, Cedar Mountain Formation, Utah: Palaios, v. 31, p. 421–439.

Kirkland, J.I., Suarez, M., Suarez, C., and Hunt-Foster, R., 2016b, The Lower Cretaceous in east-central Utah—The Cedar Mountain Formation and its bounding strata: Geology of the Intermountain West, v. 3, p. 101–228.

Lawton, T.F., 1994, Tectonic setting of Mesozoic sedimentary basins, Rocky Mountain region, United States, *in* Caputo, M.V., Peterson, J.A., and Franczyk, K.J., eds., Mesozoic systems of the Rocky Mountain region, USA: Denver, Colorado, Society of Economic Paleontologists and Mineralogists, Rocky Mountain Section, p. 1–25.

Lawton, T.F., Hunt, G.J., and Gehrels, G.E., 2010, Detrital zircon record of thrust belt unroofing in Lower Cretaceous synorogenic conglomerates, central Utah: Geology, v. 38, p. 463–466.

Lohmann, K.C., 1988, Geochemical patterns of meteoric diagenetic systems and their application to studies of paleokarst, *in* James, N.P., and Choquette, P.W., eds., Paleokarst: New York, New York, Springer-Verlag, p. 58–80.

Ludvigson, G.A., Joeckel, R.M., González, L.A., and five others, 2010, Correlation of Aptian-Albian carbon isotope excursions in continental strata of the Cretaceous foreland basin, eastern Utah, U.S.A.: Journal of Sedimentary Research, v. 80, p. 955–974.

Ludvigson, G.A., Joeckel, R.M., Murphy, L.R., and three others, 2015, The emerging terrestrial record of Aptian–Albian global change: Cretaceous Research, v. 56, p. 1–24.

Meyers, W.J., 1991, Calcite cement stratigraphy: An overview, *in* Barker, C.E., and Kopp, O.C., eds., Luminescence microscopy and spectroscopy: Qualitative and quantitative applications: Tulsa, Oklahoma, Society for Sedimentary Geology Short Course 25, p. 133–148.

Meyers, W.J., and Lohmann, K.C., 1985, Isotope geochemistry of regionally extensive calcite cement zones and marine components in Mississippian limestones, New Mexico, *in* Schneidermann, N., and Harris, P., eds., Carbonate cements: Tulsa, Oklahoma, Society for Sedimentary Geology Special Publication 36, p. 224–239.

Nelson, S.T., Heizler, M.T., and Davidson, J.P., 1992, New $^{40}Ar/^{39}Ar$ ages of intrusive rocks from the Henry and La Sal mountains, Utah: Utah Geological Survey Miscellaneous Publication 92–2, 24 p.

Paxton, S.T., Szabo, J.O., Ajdukiewicz, J., and Klimentidis, R.E., 2002, Construction of an intergranular volume compaction curve for evaluating and predicting compaction and porosity loss in rigid-grain sandstone reservoirs: American Association of Petroleum Geologists Bulletin, v. 86, p. 2,047–2,067.

Robertson, C.H., 2019, Stable isotope geochemistry and paleohydrology of the Poison Strip Sandstone, Early Cretaceous, eastern Utah [Master's thesis]: Lawrence, Kansas, University of Kansas, ProQuest Dissertations and Theses 27664011, 38 p.

Ross, J.B., Ludvigson, G.A., Schröeder-Adams, C.J., and Suarez, M.B., 2020, High latitude meteoric $\delta^{18}O$ compositions from the Cenomanian Bastion Ridge Formation, Axel Heiberg Island, Canadian Arctic Archipelago: a palaeoclimate proxy from the Sverdrup Basin, *in* Wagreich, M., Hart, M.B., Sames, B., and Yilmaz, I.O., eds., Cretaceous climate events and short-term sea-level changes: London, United Kingdom, Geological Society of London Special Publication 498, p. 57–74, https://doi.org/10.1144/SP498-2018-134.

Ross, M.L., 1998, Geology of the Tertiary intrusive centers of the La Sal Mountains, Utah—Influence of preexisting structural features on emplacement and morphology, *in* Friedman, J.D., and Huffman, A.C., Jr., eds., Laccolith complexes of southeastern Utah: Time of emplacement and tectonic setting—Workshop proceedings: U.S. Geological Survey Bulletin 2158, p. 61–83.

Spicer, R.A., and Corfield, R.M., 1992, A review of terrestrial and marine climates in the Cretaceous with implications for modeling the 'Greenhouse Earth': Geological Magazine, v. 129, p. 169–180.

Stikes, M.W., 2007, Fluvial facies and architecture of the Poison Strip Sandstone, Lower Cretaceous Cedar Mountain Formation, Grand County, Utah: Utah Geological Survey Miscellaneous Publication 06-2, 84 p.

Suarez, C.A., González, L.A., Ludvigson, G.A., and three others, 2014, Multi-taxa isotopic investigation of paleohydrology in the Lower Cretaceous Cedar Mountain Formation, eastern Utah, U.S.A.: Deciphering effects of the Nevadaplano plateau on regional climate: Journal of Sedimentary Research, v. 84, p. 975–987.

Suarez, C.A., Frucci, M.N., Tompkins, T.B., and Suarez, M.B., 2020, Quantification of a North American greenhouse hydrological cycle: using oxygen isotopic composition of phosphate from Early Cretaceous (Aptian–Albian) turtles,

in Bojar, A.-V., Pelc, A., and Lecuyer, C., eds., Stable isotope studies of the water cycle and terrestrial environments: London, United Kingdom, Geological Society of London Special Publication 507, https://doi.org/10.1144/SP507-2020-90.

Suarez, M.B., González, L.A., Ludvigson, G.A., and two others, 2009, Isotopic composition of low-latitude paleoprecipitation during the Early Cretaceous: Geological Society of America Bulletin, v. 121, p. 1,584–1,595.

Suarez, M.B., Suarez, C.A., Al-Suwaidi, A.H., and five others, 2017, Terrestrial carbon isotope chemostratigraphy in the Yellow Cat Member of the Cedar Mountain Formation: Complications and pitfalls, *in* Ziegler, K.E., and Parker, W.G., eds., Terrestrial depositional systems: Deciphering complexities through multiple stratigraphic methods: Amsterdam, the Netherlands, Elsevier, p. 303–336.

Suarez, M.B., Knight, J.A., III, Godet, A., and four others, 2020, Multiproxy strategy for determining paleoclimate parameters in the Ruby Ranch Member of the Cedar Mountain Formation, *in* Bojar, A.-V., Pelc, A., and Lecuyer, C., eds., Stable isotope studies of the water cycle and terrestrial environments: London, United Kingdom, Geological Society of London Special Publication 507, https://doi.org/10.1144/SP507-2020-85.

Ufnar, D.F., González, L.A., Ludvigson, G.A., and two others, 2002, The mid-Cretaceous water bearer: isotope mass balance quantification of the Albian hydrologic cycle: Palaeogeography, Palaeoclimatology, Palaeoecology, v. 188, p. 51–71.

Whidden, K.J., Lillis, P.G., Anna, L.O., and two others, 2014, Geology and total petroleum systems of the Paradox Basin, Utah, Colorado, New Mexico, and Arizona: The Mountain Geologist, v. 51, p.119–138.

Witke, K., Götze, J., Rössler, R., and two others, 2004, Raman and cathodoluminescence spectroscopic investigations on Permian fossil wood from Chemnitz – A contribution to the study of the permineralisation process: Spectrochimica Acta Part A: Molecular and biomolecular spectroscopy, v. 60, p. 2,903–2,912.

Wolfe, J.A., and Upchurch, G.R., Jr., 1987, North American nonmarine climates and vegetation during the Late Cretaceous: Paleogeography, Paleoclimatology, Paleoecology, v. 61, p. 33–77.

Scientific Editor: B. Ronald Frost